Stochastic Growth Bursts Enable Burden-Free Flagellum Production in a Single Bacterium

Mayra Garcia-Alcala[1] and Philippe Cluzel[1]*

[1]Department of Molecular and Cellular Biology, Harvard John A. Paulson School of Engineering and Applied Sciences, Harvard University, Cambridge, MA 02138, USA.

*Corresponding author. Email: cluzel@mcb.harvard.edu

Abstract

It is widely recognized from population-level measurements that increased production of unnecessary proteins leads to reduced bacterial growth rate, with this effect being particularly severe for flagellum synthesis. Here, we track the relationship between instantaneous growth rate variations and the activity of flagellar genes in lineages of single growing cells of E. coli. Surprisingly, we find that when flagellar gene expression is active, it is also coupled with increased growth rate. We determine that this phenomenon arises from growth bursts after divisions, which drive flagellar expression and temporarily alleviate the associated growth burden. Similar effects were observed with constitutive synthetic expression systems suggesting that an out-of-balance growth process may constitute a general strategy for mitigating the cost of expressing biosynthetically demanding genes in the single cell.

Introduction

The balance between the cost associated with expression of genes and the demand of resources imposed by growth is a fundamental and vital process for bacteria [1-4]. And recent research has established the foundation for powerful predictive frameworks [1, 4-8]. For example, at the population level, growth laws [1, 5] predict that expressing unnecessary proteins reduces the availability of ribosomes that would otherwise be destined to the synthesis of other proteins, including those involved in ribosomal function and other cellular processes. Consequently, the synthesis of those proteins is accompanied with a growth burden, which increases proportionally with the expression levels of unnecessary proteins [2, 9, 10]. Importantly, this law has been derived under the assumption of balanced-growth that refers to a state where all cellular components such as proteins, RNAs, DNA, and lipids are synthesized at rates that are proportional to the steady growth rate of the cells measured at the population level [11, 12]. Balanced-growth also ensures that the cell growth has reached a steady-state and does not run into resource bottlenecks that could impair its physiology [2, 13]. While balanced-growth is a useful assumption for predicting bacterial growth at the population level, it does not take into account out-of-balance processes [14, 15], such as sudden and stochastic growth and gene expression variation observed in the single cells [16-21], even when environmental conditions are well-controlled and steady. Therefore, extracting the laws that govern the interplay between stochastic growth variations and protein synthesis is also crucial for predicting the behavior of the single cell.

In the last few years, studies in *E. coli* have reported that flagellar genes that govern the synthesis of one of the most energy-costly bacterial organelle, exhibit large stochastic

pulses [21, 22]. The assembly of this organelle requires more than 30 different proteins that constitute the basal body of the motor and its long filament formed with ~20,000 subunits of flagellin protein (Fig. 1a). During flagellar synthesis, the cell attributes a sizable portion of the protein synthesis resources to this process [6, 23, 24]. While it has been clearly demonstrated from bulk measurements that during balanced growth, the expression of motility genes is regulated to compensate in average for the change of cell size across distinct growth conditions [25-27] a lot less is known during out-of-balance processes, such as stochastic fluctuations of growth observed at the single cell level. In view of the large protein synthesis demand that accompanies stochastic transcriptional pulses of flagellar genes, we seek to investigate how such a pulsating gene activity correlates with instantaneous growth fluctuations within a single bacterium.

The activity of flagellar genes follows a well-characterized transcriptional cascade [28]. Briefly, it begins with Class-1 genes that encode the master regulator FlhDC, which drives the transcriptional activation of Class-2 genes. These genes are involved in the synthesis of the flagellar basal body, the hook, and the alternative sigma factor, FliA. This factor, in turn, activates Class-3 genes, which encode the filament and associated signaling chemotaxis proteins (Fig. 1a). Operationally, the fact that the transcriptional activity of Class-2 and Class-3 genes flagellar genes were found to be well-delimited in time with alternating and distinct “ON” and “OFF” states, each spanning about several cellular divisions [21], makes this system experimentally accessible for identifying the relationship between temporal growth fluctuations and instantaneous flagellar gene activity in living individual cells.

Results

We track single cells growing and dividing in a microfluidic device, called 'Mother Machine' [21, 29, 30], which allows bacteria to grow exponentially under controlled conditions and over extended periods of time (Fig. 1b). This device confined cells within narrow channels, with one end exposed to a continuous flow of fresh medium and the other end sealed. The temporal activity of flagellar promoters in individual cells growing within this device was monitored using fluorescence microscopy (Material and Methods). This experimental platform enables us to capture time-lapse images and extract various physiological parameters such as cell size, elongation rate, and fluorescence signal from reporter proteins with 5 min resolution over ~27 generations (Fig. 1c, Fig. 2). One key feature of this approach is the ability to dissociate intrinsic fluctuations within the cellular system itself from its response to uncontrolled fluctuating environmental conditions.

As it was already observed by us, for wildtype *E. coli* MG1655 strain, Class-2 and 3 promoters exhibit sparse stochastic pulses while Class-1 shows low but sustained activity that resembles that of a constitutive promoter. The question then becomes how the growth rate of cells varies during distinct periods of active or inactive flagellar activity. Here we use as a proxy for growth, the elongation rate of cell size as monitored in the Mother Machine channels. And the monitor the activity of the Class-2 promoter, *fliF* using the fluorescent reporter Venus as described (see Materials and Methods) in [21]. Practically, to capture the relationship between instantaneous variations in elongation rate and Class-2 activity, we extracted them from all the time series at each time point using a Δt=5 min time window (Fig. 2 Left). The dataset formed of pairs of elongation rate-fluorescence activity are sorted by increasing activity and subsequently binned. In addition to the

wildtype MG1655 strain, we test three distinct strains whose master regulators, FlhDC, is controlled by the synthetic promoters (P1, P2, P3; [21, 31]) with increasing strength yielding increasing transcriptional activity of flagellar genes. Surprisingly, we find that for each strain, bins corresponding to the greater instantaneous transcriptional activity were also associated with the greater elongation rate (Fig. 2, Right). This result is not immediately expected as the instantaneous Activity-Elongation pair measured in the single cell is orthogonal to population-level observations where higher flagellar gene activity is associated with slower growth rate (Fig. SI1, [25-27]). This well-known population result is also recovered when we fit the bulk of the instantaneous single-cell data across the four different strains (Fig. 2, Right dashed line). The binned single-cell data demonstrate that cells with higher flagellar expression are the ones growing faster and not slower as one should expect from bulk measurements.

Next, we reasoned that if this single cell effect is indeed instantaneous, it should be also observable along individual time series and not only with binned data. To examine this point further, we exploit the fact that flagellar genes show pulses of activity, which allow us to clearly characterize between two consecutive pulses how the growth varies. In order to increase the statistics, we cut out smaller time series of Class-2 activity showing two consecutive pulses and resize their total duration to 1 (arbitrary unit) so that we can average together a large batch of these pulse-to-pulse excerpts (Fig. 3a Top; see Fig S3 and Materials and Methods). Then, we plot the time series of elongation rate and division time associated with the pulse-to-pulse excerpts. We find that the aggregated time traces of flagellar gene activity follow that of the elongation rate, while division time is in phase opposition respectively (Fig. 3a, middle and bottom). We observed that the same relations

between these variables are held for pulse-to-pulse intervals of different durations (see Fig. S3b). Finally, to further quantify the phase delay between elongation rate and Class-2 activity, we perform the cross-correlation function of the full time series (about 20 divisions) and find that fluctuations in elongation rate temporally precede those of flagellar gene activity, and they are positively correlated with each other (Fig. 3b). We repeat this analysis with the three strains whose synthetic constitutive promoters (P1, P2, P3) control the expression of the flagellum master regulator and find similar temporal delay (Fig. 3b). Since the constitutive promoters P1, P2, P3 are synthetic, they do not respond to any input specific to flagellar regulation. This latter result suggests that the observed temporal shift between flagellar activity may be driven by a global intracellular factor. Several single-cell studies have already monitored in detail the correlation between growth parameters such as the cell volume, growth rate, and the synthesis of unnecessary proteins controlled by constitutive promoters [4, 32]. Unlike the pulse-to-pulse analyses, the standard cross-correlation function alone, however, is not sufficient to tell if some specific or all time points along the Activity time series are equally likely to correlate with instantaneous variation of the elongation rate.

Next, we seek to explore whether the single cell behavior observed from our binning analyses (Fig. 2, right panel) is specific to the flagellum system or if it could be extended to more common synthetic expression systems. To this end, we repeat our binning procedure on five different strains that express the yellow fluorescent protein, Venus, under the control of synthetic constitutive promoters with different strength. Although our bulk measurements (Fig. 4a, black markers) as others [4], experimentally confirm the standard growth law—where growth rate decreases as unnecessary protein expression

increases—binning analyses of instantaneous growth rate measurements reveal a strikingly different behavior at the single-cell level. Similar to the flagellum system, our procedure shows that an instantaneous increase (decrease) in fluorescent protein synthesis is accompanied by a faster (slower) Elongation rate (Fig. 4a). Accordingly, the positive cross-correlation between Elongation rate and Activity in Figure 4b shows that growth variations precede the temporal expression fluctuations within all five strains. The result shown in Figure 4a appears to contradict the balanced-growth assumption, which posits that the increased synthesis of non-essential proteins, such as the fluorescent proteins in our experiments, depletes ribosomal availability and should consequently reduce growth rate. However, our single-cell analyses reveal a contrasting behavior, where transient growth bursts precede increases in protein synthesis. Consequently, we hypothesize that the observed behavior likely arises from an out-of-balance growth process (Fig. 4c).

Given the experimental challenges of demonstrating strict causality between transient growth bursts and instantaneous increases in protein synthesis within a living single cell, we focus on identifying the timescales of growth bursts that are deemed to be relevant to this process. To this end, we turn to the historically well-characterized strain MC4100, that has been shown to exhibit fluctuations in elongation rate at long timescales [33], much longer that the one observed in our initial wild-type MG1655 strain. As seen in Figure 5a, typical time series of the size of cells growing in the mother machine show much slower fluctuations for MC4100 than for MG1655. To quantify this difference, we plot the autocorrelation function of the time series for these two strains and find that the fluctuation timescale of size regulation is approximately 1.5 generations for MG1655, compared to

about 10 generations for MC4100 (Fig. 5b). In MG1655, the molecular origin of growth bursts are believed to arise from the asymmetric distribution of ribosomes during cell division [34, 35]. However, the molecular basis of the long-timescale fluctuations observed in MC4100 remains less clear [16, 33]. Nonetheless, our pulse-to-pulse analysis of MC4100 reveals no detectable correlation between the long-timescale bursts of growth rate and fluctuations of flagellum gene activity (Fig. 5c, top and middle panels). We reasoned that if asymmetric distribution of ribosomes [34, 36, 37], or of other intracellular factors drives short-term bursts of growth rate, such bursts should also exist in MC4100 but that they are masked by growth fluctuations at longer timescale. To test this hypothesis, we digitally subtract (Fig. 5b inset, Materials and Methods) the fluctuations at long timescale in MC4100 and then perform the pulse-to-pulse analysis, which indeed shows a similar correlation to MG1655 between the growth rate and flagellar gene activity time traces (Fig. 5c, bottom panel). Overall, these results demonstrate that only short-term growth rate fluctuations, on the timescale of a cell division, are relevant to the observed out-of-balance growth process. An additional test examining the asymmetry in growth rate distribution between two daughter cells and their corresponding flagellar gene activity immediately after division (Fig. 6) further supports the hypothesis that asymmetric distribution of intracellular factors during division, such as a surplus of ribosomes, underlies the observed out-of-balance growth process

Discussion

Kim et al. [21] found that flagellar genes in *E. coli* are activated in stochastic pulses. Subsequently, some of us proposed that these pulses were generated by means of an

inhibitor of the Class-1 transcription factor, called YdiV (RflP), which creates a monotonic ultrasensitive switch and acts as a digital filter to remove out small-amplitude input temporal fluctuations of Class-1 expression [22]. While this molecular mechanism demonstrates the possibility to generate pulses without the need of feedback, it does not propose a biological reason for the existence of the pulses. Knowing that these pulses are not an essential feature of flagellar biosynthesis, especially since some strains can be selected for or constructed to produce unregulated synthesis of flagellum with absence of pulses (such as the strain RP437 or MG1655 with insertion IS5 [21, 38]) it raises the question of the biological need of such a pulsating dynamics in wild-type strains. Here, we address this question through time series analyses to demonstrate that pulses coupled to growth bursts could transiently alleviate the burden of flagellar gene expression in the single cell. By mitigating the metabolic burden associated with the production of motility, bacteria could more effectively explore and colonize new environments. In particular, it would be especially interesting to investigate whether this advantage would be pronounced in nutrient-replete environments where rapid range expansion is crucial for survival and where seeder-bacteria with a faster growth rate would be also the ones producing flagella [39]. More generally, there have been several other important genes beside the flagellar system [18, 19, 32], which have shown pulsating dynamics. And similar time series analyses to ours may also reveal that out-of-balance growth processes serve as a general mechanism for mitigating the cost of expressing energetically expensive genes.

Materials and Methods

Strains

For a complete description of the strains see Table 2 in the Supplementary Information. Briefly: MG1655 flagella reporter strains (E98KFD and E98KFD-Pro) carry the gene for yellow fluorescent protein (mVenus NB) inserted downstream of the Class-1 native promoter of the *flhDC* operon. At the *attB* site, a Class-2 promoter *fliFp*, controls the activity of the cyan fluorescent protein SCFP3A. The strains with the constitutive promoters, the E98KFD-Pro strains, differ from E98KFD only in that the native Class-1 promoter is replaced with constitutive synthetic promoters with various strengths (P1: Pro2, P2: Pro4, P3:Pro5, from [31]). The strain construction is described in detail in [21]. Set of strains with constitutive expression of fluorescent proteins (MGPro-Venu [40]): each strain carries a low-copy plasmid with SC101 origin [41], in wich a synthetic promoter [31] controls the expression of the sequence of the mVenus NB yellow fluorescent protein [42]. We renamed the promoter according to their reported strength and measured fluorescence level (P1:Pro2, P2:Pro4, P4:ProB, P5:ProC, P6:ProD).

MC*: The classic strain MC4100 [33, 43] was modified to correct for its *flh5301* point mutation by replacing *flhD* with the same gene sequence from MG1655, and remove the insertion element IS5 upstream *flhDp*. This strain also includes a mutation to make it non-motile (MotA E98K) and carries the Class-1 and Class-2 fluorescent reporters as in the MG1655 E98KFD strains. The mutations were designed to use scarless chromosomal engineering strategy described in [21], and all transformations were performed via electroporation.

Growth Media

Microfluidic experiments were conducted using a modified version of Teknova's MOPS-EZ Medium: MOPS and Supplement EZ to 1x concentration; 0.4% glycerol serving as the carbon source, phosphate 1.32 mM. Additionally, we put surfactant (Pluronic F-108, Sigma-Aldrich) at a final concentration of 0.85 g/liter. Overnight cultures were prepared using LB medium.

Microfluidic device

We used a Mother Machine device customized for the lab set up. The master mold chip has 4 independent main feed channels where growth media flows, feeding smaller microchannels with a close end (length × width × height = 25 μm × 1.2 μm × 1.2 μm).

We fabricated the microfluidic devices by casting a 10:1 mixture of degassed PDMS and curing agent (Sylgard 184, Dow Corning) onto the mold, curing it overnight at 65 °C. The individual chips were then removed from the mold, and inlets and outlets were created using a 0.75 mm biopsy punch, then they were bonded to a glass slide (25 mm × 40 mm No. 1.5 coverglass (VWR)) using a plasma cleaner and kept it at 65 °C for another hour.

Experimental Setup

Individual colonies were cultured overnight at 30°C, then concentrated by centrifugation for 1 minute at 8000 g and loaded into the device by pipetting. After loading the device, the sample was left for 1 hour at 30°C to increase the likelihood of the cells to enter the channels by diffusion. Then the trapped cells in the channels would grow exponentially.

We flew the media through the microfluidic chamber using Tygon tubing (VWR; inside diameter 0.02 inch × outside diameter 0.06 inch), and the flow-through was collected from an outlet via a second tubing into a waste beaker. Growth medium was first pumped at a rate of 20 ul/min for at least 1 hour to allow the inlets and outlets to be cleared.

Subsequently, the flow rate was decreased to 9 µl/min, and the temperature was maintained at 30°C. We allowed approximately 3 hours for the cells to adapt before initiating the measurements.

The time-lapse images were acquired every 5 minutes on a Zeiss Axiovert 200M microscope equipped with a Plan-Apochromat 40x/1.3 Oil Ph3 Objective, a CCD camera (Hamamatsu C4742-98-24ERG) and a fluorescence excitation LED illumination source (SOLA SE II, Lumencor). We collected images from the phase contrast and epifluorescent channels (yellow, blue, and/or red protein filters, depending on the strains). The typical duration of the experiment was from 30-60 hours.

Microscopy Image Processing

We used the software BACMMAN (BACteria in Mother Machine Analyzer) [44], for cell segmentation and tracking. Using this tool, we customized various parameters to process images according to each specific strain and condition, and then manually corrected any segmentation errors.

Promoter Activity and Elongation Rate Calculations

To obtain the Elongation rate ER(t), we determined the first derivative of individual cell sizes S(t) (from birth to division) using a Savitzky–Golay filter (from Python's SciPy library)

with a window of 7 data points (35 minutes). This derivative was then normalized by dividing by the cell size, resulting in the expression $\mathrm{ER(t)} = 1/\mathrm{S(t)} \times \mathrm{dS(t)/dt}$.

We calculated Promoter Activity as $\mathrm{A(t)} = \mathrm{C(t)} \times \mathrm{ER(t)} + \mathrm{dC(t)/dt}$ from the complete time series as in [21, 32]. The concentration $\mathrm{C(t)}$ (the mean fluorescence of all the pixels that define the area of a specific cell) was smoothed with a window of 35 minutes, which we slide over the time series with an increment of 5 min. We calculated the time derivative using the Savitzky–Golay filter with a window of 35 minutes as well.

Binning

To analyze the single-cell relationship between $\mathrm{ER(t)}$ and $\mathrm{Activity(t)}$, including all the acquired time points, we first visualize it using a scatter plot. We then sort the data by creating N bins based on the value of only one of the two variables. Here we chose to sort the data using the Activity because of the clear pulsating behavior, and distinctive mean value across strains. We create the bins for them to have the same number of datapoints. Finally, foreach of these bins, we calculate the mean of both the $\mathrm{ER(t)}$ and $\mathrm{Activity(t)}$.

Pulse-to-pulse analysis

We define Class-2 pulse-to-pulse intervals, by empirically choosing a threshold to determine the *on* (above the threshold, the pulses) and off states (below the threshold). Then, for each sequence of *on-off-on* states, we identify the two maxima within the Class-2 Activity time series and extend by 15 timepoints before and after the maxima for each time interval.

We sort those intervals for them to have similar duration and rescale them from 0-1. Then we average the Class-2 Activity using a sliding window.

To examine the instantaneous relation of the pulses with other variables, we consider the same time intervals defined by the Class-2 Activity on the other time series, such as Elongation rate, Division time, etc. from the same lineages. We then rescale the intervals and use the same window size to average over their duration. The averages of these variables for different pulse-to-pulse duration intervals are presented in Fig. SI3.

Autocorrelation and Cross-Correlation Calculations

To measure the cross-correlation between $\mathrm{ER(t)}$ and $\mathrm{Activity(t)}$, we use the function 'correlate' from the signal library in Python, which evaluates how well one series matches another as a function of time displacement, lag. Prior to performing the calculation, we remove the mean from each time series. We then normalize this cross-correlation by dividing it by the square root of the product of the cross-correlation of each series with itself.

To average the cross-correlation for different lineages from the same strain, we adjust the lag by dividing it by the average division time of such series. This rescaling ensures that fluctuations due to cell division are aligned across the different series. We use the same methodology for the Autocorrelation Function.

Filtering frequencies from Size time series

To filter out the slow frequency oscillations from the Size time series in MC*, we first calculate the Power Spectral Density using Welch's method from Python's SciPy Signal

library. For every mother cell's size time series, we identify the frequency corresponding to the highest power, which we find to be *w*=0.0937 h^{-1}(~10.67 h) for all of them. We then applied to the series a notch filter for *w*, with a bandwidth of 0.01. Next calculate a new Elongation rate from the filtered series $S^{*}(t)$, by fitting an exponential function of the size of each birth-to-division event $S(t) = S_{birth} e^{ER_{*}\, t}$.

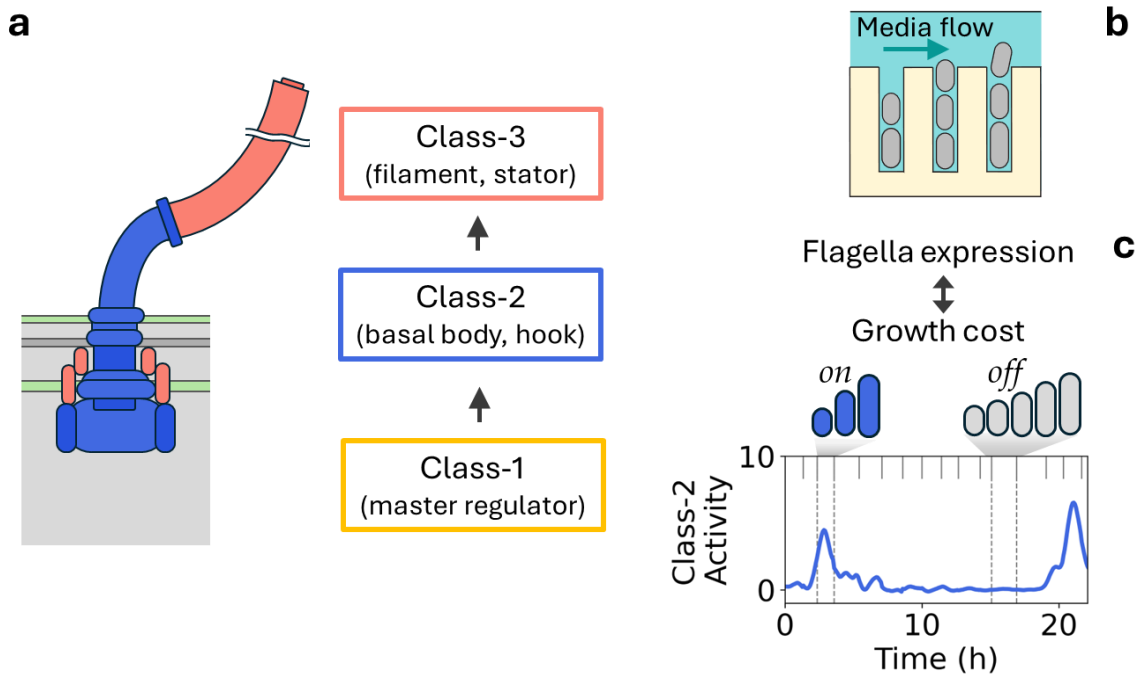

Figure 1. Monitoring simultaneously growth and transcriptional pulses of flagellar genes in single bacteria.

(**a**) Schematics of flagellar components in *E. coli*. A cascade of flagellar promoters coordinates the assembly of the different motor elements: The master regulator (Class-1) regulates the activity of Class-2 promoters that control the genes that encode the basal body and hook's molecular elements. A Class-2 gene (*fli*A) drives the transcription of the Class-3 genes which encode products needed in the late flagellar assembly, such as the filament associated proteins and the motor stator. (**b**) In the Mother Machine device, cells get constrained into channels where they can grow and divide while fed by a constant flow of fresh growth media. The 'mother' cell in the bottom of the channel is monitored over many cell divisions using an epifluorescence based time-lapse microscope. (**c**) Cells growing in the Mother Machine show bursts of Class-2 activity (*on* state) followed by long periods of no activity (*off* state) [21]. The vertical ticks show cell divisions, the dashed lines show examples of *on* and *off* states. The cartoon at the top illustrates the different growth behaviors cells exhibit during *on* and *off* states. which yields the relationship between instantaneous flagellar genes' activity and growth rate.

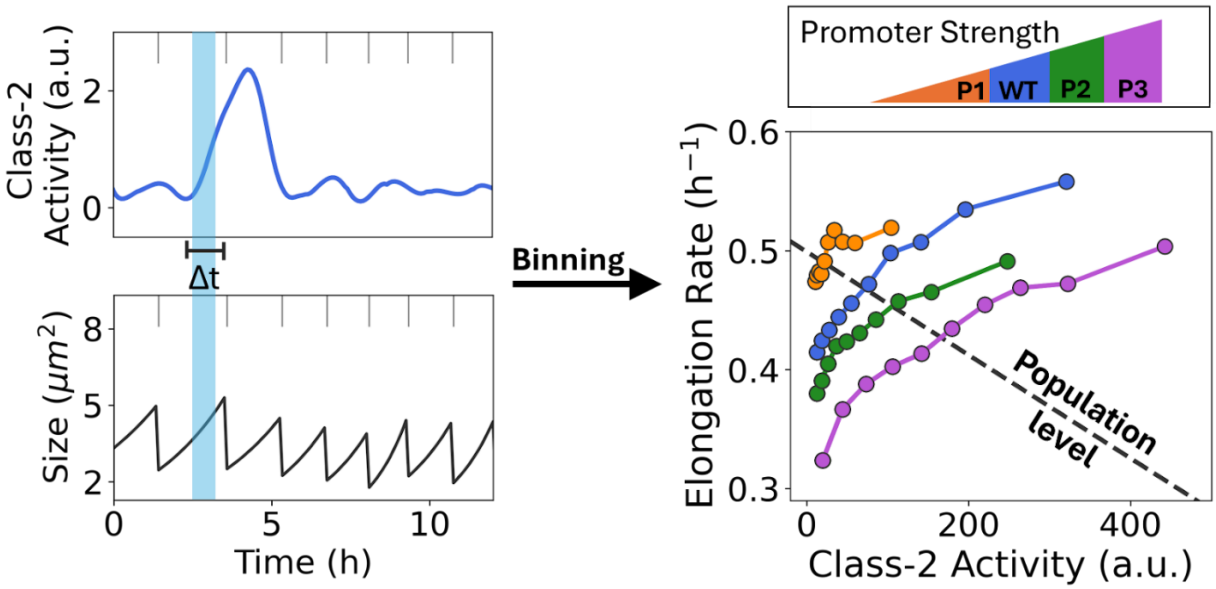

Figure 2. Relationship between instantaneous growth rate and flagellar gene activity in single cells versus population.

Left: Time traces of Class-2 Activity and Size (S) measured from the same mother cell across divisions (vertical ticks). We defined Class-2 Activity as the time derivative of total fluorescence normalized by size, and the Elongation rate as (1/S)(ΔS/Δt). First, we use Class-2 Activity to sort data points with (Δt)=5min and then binned the pair Activity-Elongation rate (see Fig. S2a). Finally, we average the data in each bin and display the result in the right panel. Because average bins are built from pairs of Activity-Elongation rate using a short time 5 minute window, it allows us to determine the relationship between instantaneous flagellar activity and growth rate in single-cells. **Right:** Instantaneous Class-2 Activity versus Elongation rate for different strains with varying mean levels of flagella expression. In such strains, the native Class-1 promoter was replaced by synthetic promoters with different strengths, P1, P2 and P3 (color coded in top panel), P3 being threefold stronger P1 [31]. The dashed line shows the linear fit to the population average of the pair Class-2 Activity-Elongation rate across strains, which illustrates the well-established relationship with a negative slope (cost) between growth rate and increasing mean flagellar activity across strains [26]. In contrast, single-cell binned data within each distinct strain shows a positive slope between instantaneous growth rate and flagellar activity demonstrating that cells with higher flagellar activity are also the ones growing faster. Only the data exhibiting Class-2 Activity (excluding *off* states) are considered in this plot; see Fig. S2b for all states. The number of time traces are n=(69, 107, 96, 67) for the strains with the promoter P1, WT, P2, P4, respectively, all with a similar duration of 47 hours.

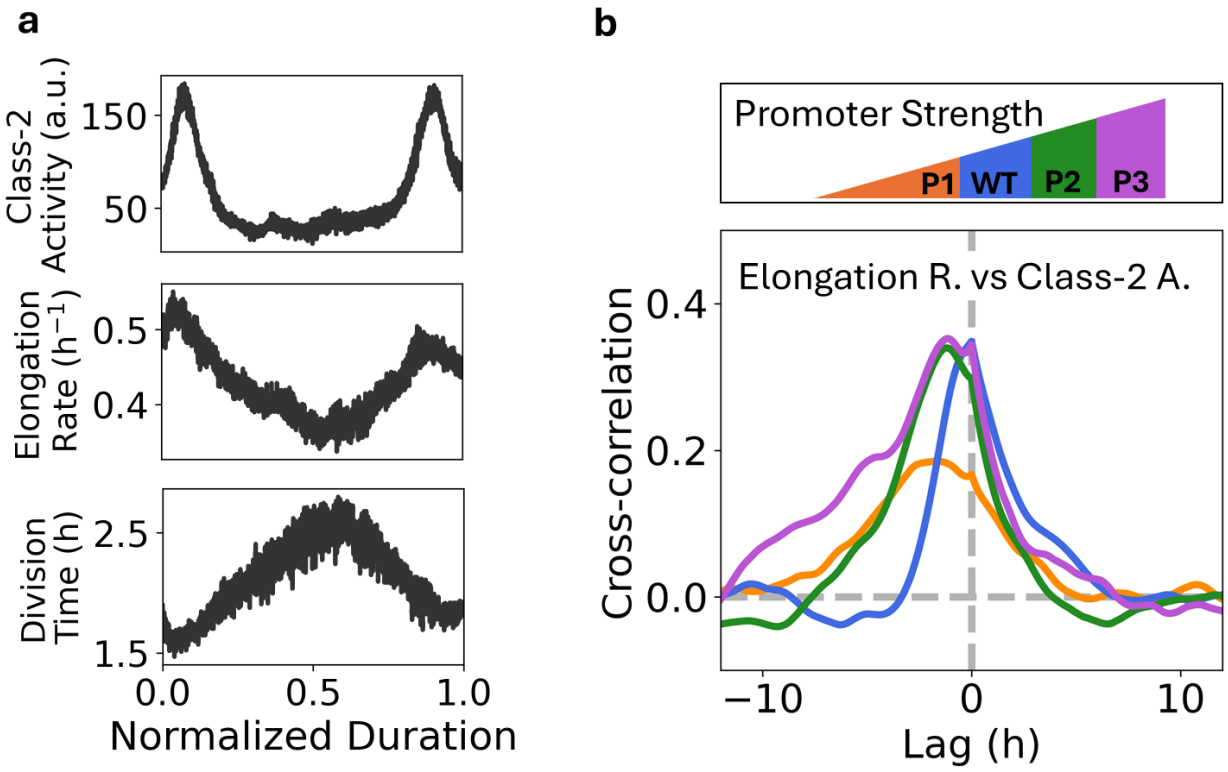

Figure 3. Cells grow faster during pulses.

(**a**) Top: Averaged pulse-to-pulse intervals (real time is rescaled to 1) of two successive pulses of Class-2 Activity in a strain with the native wild-type flagellar expression (strain EMGFD; n=103 intervals); middle and bottom: Elongation rate and division time associated with the same time intervals as top panel (See Materials and Methods and Fig S3). (**b**) Cross-correlation functions of Elongation rate and Class-2 Activity across strains with different flagellar transcriptional activity. Individual cross-correlation functions are computed for each time series (lineages) for each strain and then averaged together. The colored curves represent cross-correlation functions for the different strains with increasing strength of the Class-1 synthetic promoter ranging from P1 to P3 as indicated by the color panel. The number of time traces are n=(69, 107, 96, 67) for the strains with the promoter P1, WT, P2, P4, respectively, all with a similar duration of 47 hours.

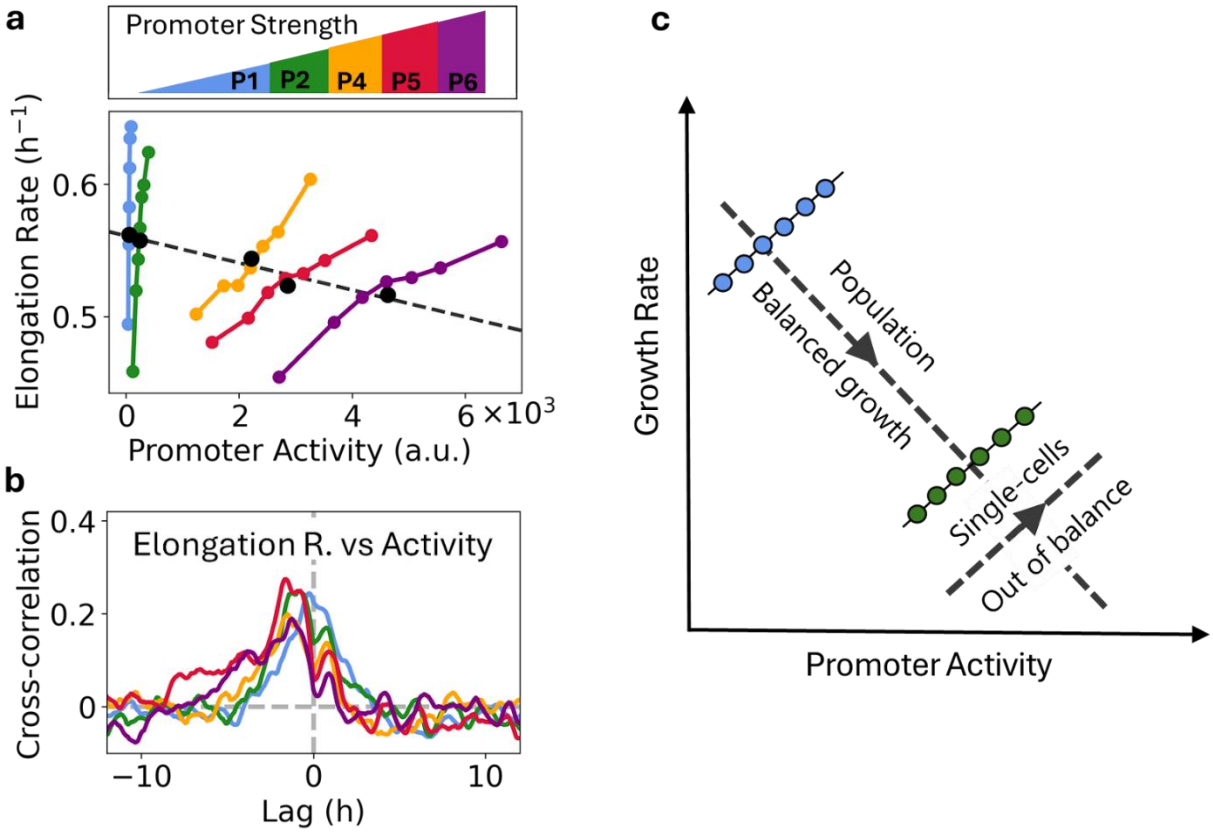

Figure 4. Relationship between instantaneous growth and Promoter Activity in single-cells versus population for different levels of constitutive expression of unnecessary proteins.

(**a**) For a set of strains expressing the fluorescent protein Venus, driven by promoters of varying strengths (P1,...,P6, as indicated at the top), we calculated the mean Elongation rate as a function of binned Promoter Activity. The black dots represent the average for the entire population of each strain, while the line indicates the linear fit of these points. In each strain, cells exhibit a positive correlation between Elongation rate and the constitutive Promoter Activity. (**b**) The average cross-correlation between Elongation rate and Promoter Activity was calculated for the lineages of strains producing unnecessary proteins (same data and color-coding as in panel (**a**)). For each strain, the binning and cross-correlation were computed for n = (30, 21, 19, 14, 24) lineages for the strains with promoters P1 through P6, respectively, each time series with an approximate duration of 37 hours. (**c**) Schematic representation of binned data that yields the relationship between instantaneous (Δt= 5 min) promoter activity and out-of-balance growth. In each different strain (blue and green) instantaneous behavior is orthogonal to the common population behavior for which synthesis of unnecessary proteins is accompanied by a decrease of growth rate.

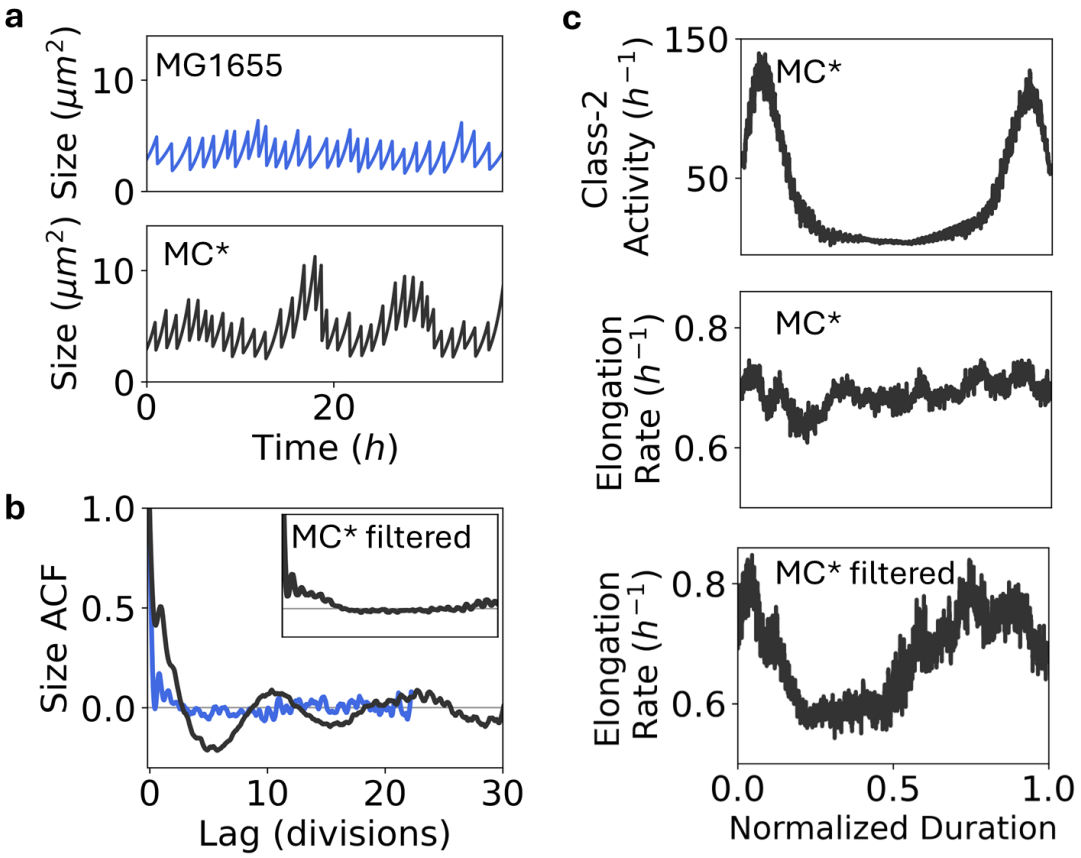

Figure 5. Long timescale growth fluctuations spanning many divisions are not correlated with flagellar biosynthesis pulses, but shorter timescale (~1.5 division) growth fluctuations are.

(**a**) Typical time series showing the Size of an MG1655 background stain (top) and MC* (motile variant of MC4100). (**b**) Autocorrelation Function (ACF) of the Size, S(t) time series in MG1655 (blue) and long-term fluctuating MC* strain (black). Averages of individual ACF were calculated from ~60 lineages and normalized by the mean division time. **Inset**: Average ACF of the MC* Size time series that were digitally filtered to remove the long time scale frequencies (~10 generations; see Materials and Methods). (**c**) **Top**: Mean Class-2 Activity of peak-to-peak intervals of Activity time traces in MC*. These intervals were normalized to yield a total duration of 0-1. **Middle**: for the same time intervals as in Top, mean Elongation rate. **Bottom**: Mean Elongation rate calculated using filtered Size time series in MC*, which shows that only short-time scale and not long-time scale growth fluctuations drive growth fluctuations (n=40 intervals).

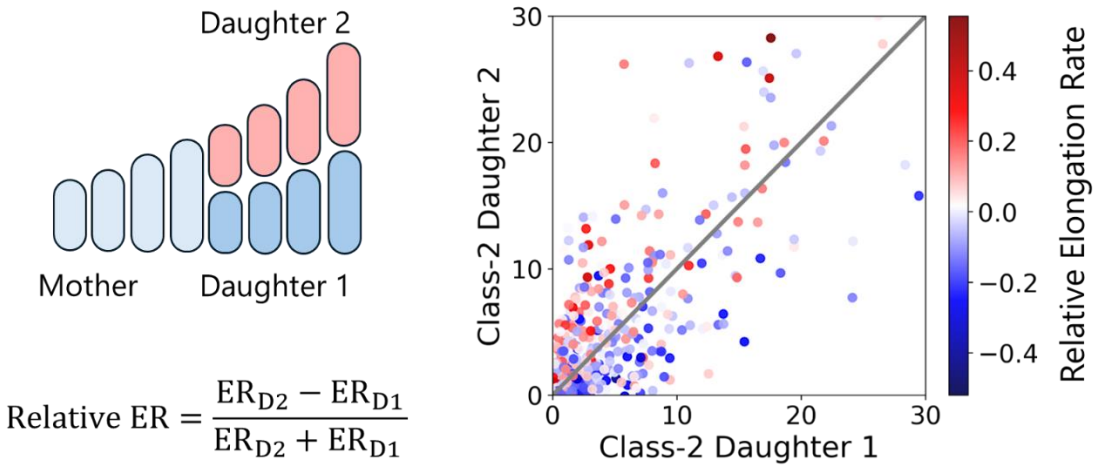

Figure 6. Comparison of daughter cells' Elongation rate and pulsatile Class-2 Activity.

The schematic representation (left) illustrates the growth of a mother cell, which divides to produce two daughter cells, Daughter 1 and Daughter 2. For each daughter cell from the MG1655 background strain, E98KFD, we calculated the Elongation rate (ER) as the exponent that best fits the daughters' cell size over time from birth to division using the formula $S(t) = S_{birth}e^{\mathrm{ER}*t}$. To compare the elongation rates of the two daughter cells, we computed the Relative Elongation rate, as defined in the figure. If the Elongation rate of Daughter 2 (ER2) is larger than that of Daughter 1 (ER1), the Relative ER is greater than 1. Conversely, if ER2 is lower than ER1, the relative ER is less than 1, and if both have the same ER, its value is 0. Additionally, we determined the daughter's Class-2 Activity by measuring the change in fluorescence divided by the division time. The scatter plot (right) corresponds to the Class-2 Activity for both daughters. The diagonal line indicates equal promoter activity between the two daughter cells. The data points are color-coded: blue if ER1>ER2, red if ER2>ER1, which shows on average that when one of the daughters has higher flagella expression than the other, it also elongates faster (n=541, daughters cells; ER1 = 0.544 ± 0.176 h^{-1}, ER2 = 0.539 ± 0.168 h^{-1}).

Acknowledgments

We thank Maximino Aldana and Mark Kim for early discussions and advice, and the Cluzel lab members for critical reading of the manuscript. **Funding:** This work was performed, in part, at the Center for Nanoscale Systems (CNS), a member of the National Nanotechnology Infrastructure Network (NNIN), which is supported by the NSF under award no. ECS-0335765. CNS is part of Harvard University. This work was supported by grant 1615487 from the NSF.

References

[1] M. Scott and T. Hwa, "Bacterial growth laws and their applications," *Current Opinion in Biotechnology,* vol. 22, no. 4, pp. 559-565, 2011, doi: 10.1016/j.copbio.2011.04.014.

[2] E. Dekel and U. Alon, "Optimality and evolutionary tuning of the expression level of a protein," vol. 436, no. July, pp. 588-592, 2005, doi: 10.1038/nature03842.

[3] D. M. Stoebel, A. M. Dean, and D. E. Dykhuizen, "The cost of expression of Escherichia coli lac operon proteins is in the process, not in the products," *Genetics,* vol. 178, no. 3, pp. 1653-1660, 2008/3// 2008, doi: 10.1534/genetics.107.085399.

[4] M. Basan *et al.*, "Inflating bacterial cells by increased protein synthesis," *Molecular Systems Biology,* vol. 11, no. 10, pp. 836-836, 2015, doi: 10.15252/msb.20156178.

[5] M. Scott, C. W. Gunderson, E. M. Mateescu, Z. Zhang, and T. Hwa, "Interdependence of Cell Growth," *Science,* vol. 330, no. November, pp. 1099-1102, 2010, doi: 10.1126/science.1192588.

[6] D. W. Erickson, S. J. Schink, V. Patsalo, J. R. Williamson, U. Gerland, and T. Hwa, "A global resource allocation strategy governs growth transition kinetics of Escherichia coli," *Nature,* 2017, doi: 10.1038/nature24299.

[7] M. Scott, S. Klumpp, E. M. Mateescu, and T. Hwa, "Emergence of robust growth laws from optimal regulation of ribosome synthesis," *Molecular Systems Biology,* vol. 10, no. 8, pp. 747-747, 2014, doi: 10.15252/msb.20145379.

[8] L. Pacciani-Mori, S. Suweis, A. Maritan, and A. Giometto, "Constrained proteome allocation affects coexistence in models of competitive microbial communities," *The ISME Journal,* vol. 15, no. 5, pp. 1458-1477, 2021, doi: 10.1038/s41396-020-00863-0.

[9] H. Dong, L. Nilsson, and C. G. Kurland, "Gratuitous overexpression of genes in Escherichia coli leads to growth inhibition and ribosome destruction," *Journal of Bacteriology,* vol. 177, no. 6, pp. 1497-1504, 1995, doi: 10.1128/jb.177.6.1497-1504.1995.

[10] I. Shachrai, A. Zaslaver, U. Alon, and E. Dekel, "Cost of Unneeded Proteins in E. coli Is Reduced after Several Generations in Exponential Growth," *Molecular Cell,* vol. 38, no. 5, pp. 758-767, 2010, doi: 10.1016/j.molcel.2010.04.015.

[11] S. Klumpp, Z. Zhang, and T. Hwa, "Growth Rate-Dependent Global Effects on Gene Expression in Bacteria," *Cell,* vol. 139, no. 7, pp. 1366-1375, 2009, doi: 10.1016/j.cell.2009.12.001.

[12] S. Klumpp and T. Hwa, "Growth-rate-dependent partitioning of RNA polymerases in bacteria," *Proceedings of the National Academy of Sciences of the United States of America,* vol. 105, no. 51, pp. 20245-20250, 2008, doi: 10.1073/pnas.0804953105.

[13] H. Dourado and M. J. Lercher, "An analytical theory of balanced cellular growth," *Nature Communications,* vol. 11, no. 1, 2020, doi: 10.1038/s41467-020-14751-w.

[14] Y. Korem Kohanim, D. Levi, G. Jona, B. D. Towbin, A. Bren, and U. Alon, "A Bacterial Growth Law out of Steady State," *Cell Reports,* vol. 23, no. 10, pp. 2891-2900, 2018, doi: 10.1016/j.celrep.2018.05.007.

[15] T. Bollenbach, S. Quan, R. Chait, and R. Kishony, "Nonoptimal Microbial Response to Antibiotics Underlies Suppressive Drug Interactions," *Cell,* vol. 139, no. 4, pp. 707-718, 2009/11// 2009, doi: 10.1016/j.cell.2009.10.025.

[16] K. Biswas, A. E. Sanderson, H. Salman, and N. Brenner, "Single-cell Growth Rate Variability in Balanced Exponential Growth," *bioRxiv,* p. 2024.06.23.600237, 2024, doi: 10.1101/2024.06.23.600237.

[17] J. Park *et al.*, "Molecular Time Sharing through Dynamic Pulsing in Single Cells," *Cell Systems,* vol. 6, no. 2, pp. 216-229.e15, 2018, doi: 10.1016/j.cels.2018.01.011.

[18] O. Patange *et al.*, "Escherichia coli can survive stress by noisy growth modulation," *Nature Communications,* vol. 9, no. 1, 2018, doi: 10.1038/s41467-018-07702-z.

[19] E. C. Jones and S. Uphoff, "Single-molecule imaging of LexA degradation in Escherichia coli elucidates regulatory mechanisms and heterogeneity of the SOS response," *Nature Microbiology,* vol. 6, no. 8, pp. 981-990, 2021/08/01 2021, doi: 10.1038/s41564-021-00930-y.

[20] S. Goldman, M. Aldana, and P. Cluzel, "Resonant learning in scale-free networks," *PLOS Computational Biology,* vol. 19, no. 2, p. e1010894, 2023, doi: 10.1371/journal.pcbi.1010894.

[21] J. Mark Kim, M. Garcia-Alcala, E. Balleza, and P. Cluzel, "Stochastic transcriptional pulses orchestrate flagellar biosynthesis in Escherichia coli," *Science Advances,* vol. 6, no. 6, 2020, doi: 10.1126/sciadv.aax0947.

[22] A. S. Sassi, M. Garcia-Alcala, M. J. Kim, P. Cluzel, and Y. Tu, "Filtering input fluctuations in intensity and in time underlies stochastic transcriptional pulses without feedback," *Proceedings of the National Academy of Sciences of the United States of America,* vol. 117, no. 43, pp. 26608-26615, 2020, doi: 10.1073/pnas.2010849117.

[23] M. Mori *et al.*, "From coarse to fine: the absolute Escherichia coli proteome under diverse growth conditions," *Molecular Systems Biology,* vol. 17, no. 5, pp. 1-23-23, 2021/05/01 2021, doi: 10.15252/msb.20209536.

[24] P. E. Schavemaker and M. Lynch, "Flagellar energy costs across the tree of life," *eLife,* vol. 11, 2022, doi: 10.7554/ELIFE.77266.

[25] T. Honda, J. Cremer, L. Mancini, Z. Zhang, T. Pilizota, and T. Hwa, "Coordination of gene expression with cell size enables Escherichia coli to efficiently maintain motility across conditions," doi: 10.1073/pnas.

[26] B. Ni, R. Colin, H. Link, R. G. Endres, and V. Sourjik, "Growth-rate dependent resource investment in bacterial motile behavior quantitatively follows potential benefit of chemotaxis," *Proceedings of the National Academy of Sciences of the United States of America,* vol. 117, no. 1, pp. 595-601, 2020, doi: 10.1073/pnas.1910849117.

[27] B. Ni, B. Ghosh, F. S. Paldy, R. Colin, T. Heimerl, and V. Sourjik, "Evolutionary Remodeling of Bacterial Motility Checkpoint Control," *Cell Reports,* vol. 18, no. 4, pp. 866-877, 2017, doi: 10.1016/j.celrep.2016.12.088.

[28] D. M. Fitzgerald, R. P. Bonocora, and J. T. Wade, "Comprehensive Mapping of the Escherichia coli Flagellar Regulatory Network," *PLoS Genetics,* vol. 10, no. 10, 2014, doi: 10.1371/journal.pgen.1004649.

[29] P. Wang *et al.*, "Robust growth of escherichia coli," *Current Biology,* vol. 20, no. 12, pp. 1099-1103, 2010, doi: 10.1016/j.cub.2010.04.045.
[30] J. R. Moffitt, J. B. Lee, and P. Cluzel, "The single-cell chemostat: an agarose-based, microfluidic device for high-throughput, single-cell studies of bacteria and bacterial communities," *Lab on a Chip,* vol. 12, no. 8, pp. 1487-1487, 2012, doi: 10.1039/c2lc00009a.
[31] J. H. Davis, A. J. Rubin, and R. T. Sauer, "Design, construction and characterization of a set of insulated bacterial promoters," *Nucleic Acids Research,* vol. 39, no. 3, pp. 1131-1141, 2011, doi: 10.1093/nar/gkq810.
[32] N. M. V. Sampaio, C. M. Blassick, V. Andreani, J.-B. Lugagne, and M. J. Dunlop, "Dynamic gene expression and growth underlie cell-to-cell heterogeneity in Escherichia coli stress response," 2022, doi: 10.1073/pnas.
[33] Y. Tanouchi *et al.*, "A noisy linear map underlies oscillations in cell size and gene expression in bacteria," *Nature,* vol. 523, no. 7560, pp. 357-359, 2015, doi: 10.1038/nature14562.
[34] J. H. van Heerden, A. Berkvens, D. H. de Groot, and F. J. Bruggeman, "Growth consequences of the inhomogeneous organization of the bacterial cytoplasm," ed: eLife Sciences Publications, Ltd, 2024.
[35] L. Chao, C. K. Chan, C. Shi, and U. C. Rang, "Spatial and temporal distribution of ribosomes in single cells reveals aging differences between old and new daughters of Escherichia coli," *eLife,* vol. 12, p. RP89543, 2024/11/20 2024, doi: 10.7554/eLife.89543.
[36] Q. Chai *et al.*, "Organization of ribosomes and nucleoids in escherichia coli cells during growth and in quiescence," *Journal of Biological Chemistry,* vol. 289, no. 16, pp. 11342-11352, 2014, doi: 10.1074/jbc.M114.557348.
[37] S. Bakshi, H. Choi, and J. C. Weisshaar, "The spatial biology of transcription and translation in rapidly growing Escherichia coli," *Frontiers in Microbiology,* Review vol. 6, 2015, doi: 10.3389/fmicb.2015.00636.
[38] C. S. Barker, B. M. Prüß, and P. Matsumura, "Increased motility of Escherichia coli by insertion sequence element integration into the regulatory region of the flhD operon," *Journal of Bacteriology,* vol. 186, no. 22, pp. 7529-7537, 2004, doi: 10.1128/JB.186.22.7529-7537.2004.
[39] J. Cremer, T. Honda, Y. Tang, J. Wong-Ng, M. Vergassola, and T. Hwa, "Chemotaxis as a navigation strategy to boost range expansion," *Nature,* vol. 575, no. 7784, pp. 658-663, 2019/11// 2019, doi: 10.1038/s41586-019-1733-y.
[40] A. S. Sassi, M. Garcia-Alcala, M. Aldana, and Y. Tu, "Protein Concentration Fluctuations in the High Expression Regime: Taylor's Law and Its Mechanistic Origin," *Physical Review X,* vol. 12, no. 1, 2022/3// 2022, doi: 10.1103/PhysRevX.12.011051.
[41] R. Lutz and H. Bujard, "Independent and tight regulation of transcriptional units in escherichia coli via the LacR/O, the TetR/O and AraC/I1-I2 regulatory elements," *Nucleic Acids Research,* vol. 25, no. 6, pp. 1203-1210, 1997, doi: 10.1093/nar/25.6.1203.
[42] E. Balleza, J. M. Kim, and P. Cluzel, "Systematic characterization of maturation time of fluorescent proteins in living cells," *Nature Methods,* vol. 15, no. 1, pp. 47-51, 2018, doi: 10.1038/nmeth.4509.
[43] J. E. Peters, T. E. Thate, and N. L. Craig, "Definition of the Escherichia coli MC4100 genome by use of a DNA array," *Journal of Bacteriology,* vol. 185, no. 6, pp. 2017-2021, 2003/3// 2003, doi: 10.1128/JB.185.6.2017-2021.2003.
[44] J. Ollion, M. Elez, and L. Robert, "High-throughput detection and tracking of cells and intracellular spots in mother machine experiments," *Nature Protocols,* vol. 14, no. 11, pp. 3144-3161, 2019, doi: 10.1038/s41596-019-0216-9.